European Review for Medical and Pharmacological Sciences 2023; 27: 3622-3630

Cellular density and variability in laryngeal and pharyngeal squamous cell carcinoma using confocal laser endomicroscopy

M. SIEVERT[1], M. AUBREVILLE[2], M. ECKSTEIN[3], K. MANTSOPOULOS[1], M. KOCH[1], A.O. GOSTIAN[1], S.K. MUELLER[1], H. IRO[1], M. GONCALVES[4]

[1]Department of Otorhinolaryngology, Friedrich-Alexander-Universität Erlangen-Nürnberg, Head and Neck Surgery, University Hospital, Erlangen, Germany
[2]Technische Hochschule Ingolstadt, Ingolstadt, Germany
[3]Institute of Pathology, Friedrich-Alexander-Universität Erlangen-Nürnberg, University Hospital, Erlangen, Germany
[4]Department of Otorhinolaryngology, Head and Neck Surgery, Rheinische Westfälische Technische Hochschule Aachen, University Hospital, Aachen, Germany

Abstract. – OBJECTIVE: Confocal laser endomicroscopy (CLE) allows the visualization of epithelium in a thousand-fold magnification. This study analyzes the architectural differences at the cellular level of the mucosa and squamous cell carcinoma (SCC).

PATIENTS AND METHODS: A total of 60 CLE sequences recorded in 5 patients with SCC undergoing laryngectomy between October 2020 and February 2021 were analyzed. The corresponding histologic sample derived from H&E staining was assigned to each sequence, capturing CLE images of the tumor and healthy mucosa. In addition, the cellular structure analysis was performed to diagnose SCC by measuring the total number of cells and cell size in 60 sequences in a fixed field of view (FOV) with 240 µm in diameter (45,239 µm²).

RESULTS: Out of 3,600 images, 1,620 (45%) showed benign mucosa and 1,980 (55%) SCC. The automated analysis yielded a difference in cell size, with healthy epithelial cells being 171.9±82.0 µm² smaller than SCC cells, which were 246.3±171.9 µm² and showed greater variability in size (p=0.037). In addition, due to the probe's fixed FOV, there was a difference in cell count with a total of 188.7±38.3 and 124.8±38.6 cells in images of normal epithelium and SCC (p<0.001), respectively. Regarding cell density as a criterion for the differentiation of benign/malign, using a cut-off value of 145.5 cells/FOV, we obtained sensitivity and specificity of 88.0% and 71.9%, respectively.

CONCLUSIONS: SCC reveals marked differences at a cellular level compared to the healthy epithelium. Our results further support the importance of this feature for identifying SCC during CLE imaging.

Key Words:
Head and neck squamous cell carcinoma, Confocal laser endomicroscopy, Classification, Optical biopsy, Larynx, Pharynx.

Introduction

The larynx is located on the transition of the digestive and respiratory tracts. Its intact function enables the primary functions of breathing and swallowing and the secondary function of vocalization. Microscopical, histopathological assessment of the tissue is still the gold standard for diagnosing and managing laryngeal cancer[1,2]. Especially in small, delicate anatomical regions such as the vocal cords, even small tissue excisions can cause irreversible voice disorders[3]. The goal of complete oncological resection without over-sampling tumor margins to preserve as much function as possible is a balancing act, which could be served by non-invasive, reliable, and precise "optical biopsy". Therefore, various non-invasive optical imaging methods have emerged in the last decade as potential alternatives to tissue biopsy, albeit mostly in experimental settings[4-8]. Confocal laser endomicroscopy (CLE) is a promising imaging technology that provides a magnified, cellular-level view of superficial epithelium[9]. CLE utilizes a small laser scanning probe applied to the area of interest. A fixed 600 µm field of view enables a 1,000 times magnification for real-time visualization of the superficial tissue architecture[10]. Fluore-

Corresponding Author: Miguel Goncalves, Ph.D; e-mail: mgoncalves@ukaachen.de

scein enables outlining the intercellular spaces and visualization of blood vessels and provides "real-time" optical biopsies[11]. Acquired images comprise histopathologic tangential sections of the tissue at the depth defined by the specific probe. A reliable classification and diagnosis of abnormal and normal tissue is non-trivial, requires specific knowledge, and is supported by classification systems[12-14]. In these classification systems, capillary aberrations, tissue homogeneity, cell size, and cell delineation play a significant role[15,16]. Similarly to capillary aberrations and tissue inhomogeneity, which were studied in previous publications[12-16], cell density, shape, and size are integral to all classification systems. Although an 80-90% accuracy is reported in earlier publications, examiner-dependency remains a major problem to the broad implementation of this technique[12,13]. Therefore, an objective, independent examination of these parameters is very important. The cell architecture seems to be a reliable indicator of malignancy in most cases, although an objective analysis of this parameter has not been performed to our knowledge regarding CLE. We hypothesize that even in the small area corresponding to the diameter of the probe, SCC has a quantifiable difference in cell density and size that correlates with histology and is different from normal squamous cell epithelium. This study aimed to assess the differences in cell density (number of cells in the fixed field of view) and cell size between healthy epithelium and SCC in CLE images.

Patients and Methods

Study Design

We conducted this prospective pilot study at a tertiary department of otorhinolaryngology, head and neck surgery, an academic cancer center. The local Institutional Ethics Committee approved this study (approval number 60_14 B), following Helsinki Declaration. Written informed consent was obtained from all study participants.

Eligibility Criteria

In total, five consecutively diagnosed patients with SCC of the larynx or pharynx were included in this study. The exclusion criteria were previous treatment for cancer, distant metastases, radiation to the head and neck, pregnancy, thyroid dysfunction, minority, severe kidney failure, and allergy to Fluorescein.

Confocal Laser Endomicroscopy Procedure

We performed intraoperative data acquisition using a GastroFlex probe and a 488 nm Cellvizio™ 100s device (Mauna Technologies, Paris, France). The GastroFlex™ probe has a diameter of 2.6 mm, enabling a penetration depth of 55-65 µm in a 240 µm field of view. It has a resolution of approximately 1 µm. As an optical dye, we used 5 ml of Fluorescein, 10% (Alcon Pharma GmbH, Freiburg, Germany). The first step was the elevation of the apron flap, following mobilization of the larynx. We subsequently performed a pharyngotomy. The exposure of the tumor was followed by the CLE examination. Next, 5 ml Fluorescein Alcon 10% (Alcon Pharma GmbH, Freiburg, Germany) was injected intravenously. The CLE probe obtained images of the tumor- and incision margin. The scanned areas were then marked with sutures, or separate biopsies of the exact location of the image acquisition were taken. This allowed us to correlate imaging data with the gold standard of histopathology. The histopathological assessments followed a standard protocol using hematoxylin and eosin (H&E) staining. After completing the imaging, we performed complete tumor resection. Therefore, neither our nor international standards of care were altered or affected by using CLE.

Annotation Process

Sequences were analyzed using ImageJ Analysis software (NHI, Bethesda, Maryland, USA). First, we selected a representative image from each test sequence that was free of artifacts and contamination of the probe with blood or saliva. Next, all images were categorized as malignant or benign using the reference standard of histopathological analysis. To determine the size of the cells, we marked a measurement area of 20 µm in each image as a reference. The image was then extracted and cropped to a field of view of 240 µm. After subtracting the background and adjusting the threshold, the 16-bit image was counted using watershed processing and particle analysis (Figure 1). The threshold was adjusted to exclude the edges of the image. Therefore, a minimum particle size of 40 μm^2 was defined. The image processing was done the same for all 60 sequences to ensure the highest level of comparability.

Statistical Analysis

The two-tailed *t*-test for independent samples was applied to compare each mean value and standard deviation (SD). A *p*-value lower than $p<0.05$

was considered statistically significant. We performed statistical analysis using SPSS version 26.0 for Windows (IBM Corp., Armonk, NY, USA).

Results

Patient Cohort

Between March 2020 and February 2021, we enrolled five patients (all males; mean age 65.4 years (SD = 11.9) to undergo *in vivo* CLE during planned transcervical tumor resection concerned with the hypopharynx and larynx. The tumor resection was performed *via* an open approach in each case. In one patient (20%), the tumor was located in the larynx. Four patients (80%) also presented with hypopharyngeal mucosa involvement. Microvascular defect reconstruction was necessary in three cases (60%). Regarding the tumor grading, one patient (20%) has an intermediate grade (G2), and four patients (80%) have poor grade differentiation (G3). Patient characteristics, including stage, are presented in Table I. In all cases, safe margin resection could be performed independently of CLE use. Circular margin specimens in the intraoperative frozen section defined in sano resection. We confirmed a safety margin of >0.5 cm in all patients.

Sequence Selection

Out of 12,065 images, 60 sequences (3,600 images; 33 sequences of SCC and 27 sequences of benign mucosa) were selected and evaluated as representative in acceptable quality. We matched each of these sequences (60 images, 5 seconds) with a corresponding sample by H&E staining to determine the diagnostic accuracy. All benign mucosal specimens excluded dysplasia or carcinoma *in situ*. The mean image acquisition time was 5 minutes (SD=1.3) for each patient, supplemented by the assembly and disassembly of the scan unit of approximately 5 minutes.

Cellular Structure in Benign and Malignant Mucosa

The results of the automated image-based cell counting and surveying are shown in Table II. There was a significant difference, with a

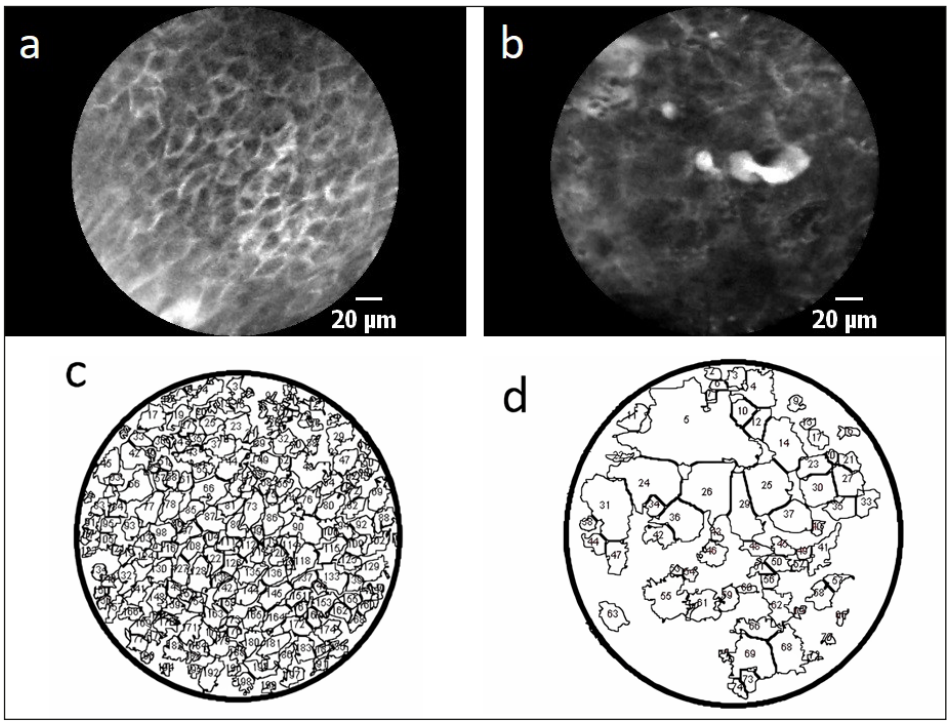

Figure 1. Example of Automated Image Analysis. In the upper section, we see the CLE images of normal squamous epithelium (**a**) and the squamous cell carcinoma (**b**) with the corresponding sequencing in the lower section (**c-d**). Noticeably, blurred cell borders and cell conglomerates in squamous cell carcinomas (**b**) are reflected in a lower total cell count (74 cells *vs.* 199 cells) with cells of different sizes (**d**). In addition, cell connectivity is disrupted by dilated capillaries and vascular leakage.

Table I. Characteristics of patient cohort..

Case No.	Age (years)	Tumor Stage	Location	Grade	Surgery	CLE frames (n)	Recording time (seconds)	Selected sequences (n)
1.	71	T4a	Larynx Hypopharynx	G3	Total LE, partial pharyngectomy	1,468	183	14
2.	56	T4a	Larynx Hypopharynx	G3	Total LE, partial pharyngectomy	2,204	275	12
3.	86	T4a	Larynx	G2	Total LE	2,191	273	10
4.	61	T2	Larynx Hypopharynx	G3	Total LE, partial pharyngectomy	3,311	413	14
5.	53	T3	Larynx Hypopharynx	G3	Total LE, partial pharyngectomy	2,891	361	10
				Total		12,065	1,505	60

LE - laryngectomy.

Table II. Cell count and measurement.

	Squamous epithelium	Squamous cell carcinoma	*p*-value	Total
Number of counted cells (n; mean ± SD)	188.7±38.3	124.8±38.6	<0.001	152.8±49.8
Number of counted cells (n; range)	125-277	34-223	-	34-277
Cell size (μm^2; mean±SD)	171.9±82.0	246.3±171.9	0.037	213.6±143.6
Cell size (μm^2; range)	57.4-338.5	42.3-587.9	-	42.3-587.9

SD = Standard deviation.

total of 188.7±38.3 cells in images of normal epithelium and 124.8±38.6 cells in SCC per FOV (p<0.001; Figure 2). It is worth mentioning that it is only the cell count in the image field of view and not a general cell proliferation, as it is familiar with malignant tissue. Regarding the cell size in each image, there is also a significant difference in images of SCC and the normal squamous epithelium and the SCC with a mean area of 246.3±171.9 μm^2 and 171.9±82.0 μm^2, respectively (p=0.037). In addition, with a mean SD of 354.1±339.4 μm^2 and 162.2±121.0 μm^2, there is a significantly higher variance regarding cell size in images of SCC compared to the normal epithelium (p=0.005) (Figure 3).

Receiver Operating Characteristic Curve Analysis of the Cell Density

Considering the cell density, i.e., the number of cells pro fixed field of view with 240 µm in diameter (=45,239 μm^2; FOV), we obtained a significant difference in the benign and malignant epithelium, as noted above). A ROC curve was plotted subsequently for cell density in SCC and healthy tissue to determine a cut-off value of the highest sensitivity and specificity (Figure 4).

An area under the curve (AUC) was calculated with 87.6 (95% CI 78.9-96.4). A cut-off value between the two groups was defined as 145.5 cells/FOV (Table III). Sensitivity and specificity using a cut-off value were 136.5 cells/FOV 96.0% and 65.6%, respectively. Sensitivity and specificity using a cut-off value of 145.5 cells/FOV 88.0%, and 71.9%, respectively.

Discussion

This study evaluated the cell count per field of view (cell density) and cell size in the confocal laser microscopic examination of laryngeal carcinomas. Carcinoma's important histological features generally include epithelial tumor cells

Table III. Diagnostic metrics depend on cell density to identify malignancy as a stand-alone criterion–selected points in the ROC.

Cell count per field of view (260 µm diameter, 45,239 μm^2)	Sensitivity	Specificity
121.0	100%	53.1%
136.5	**96.0%**	**65.6%**
145.5	**88.0%**	**71.9%**
157.0	**72.0%**	**81.2%**
175.0	64.0%	93.7%
203.0	40%	96.9%

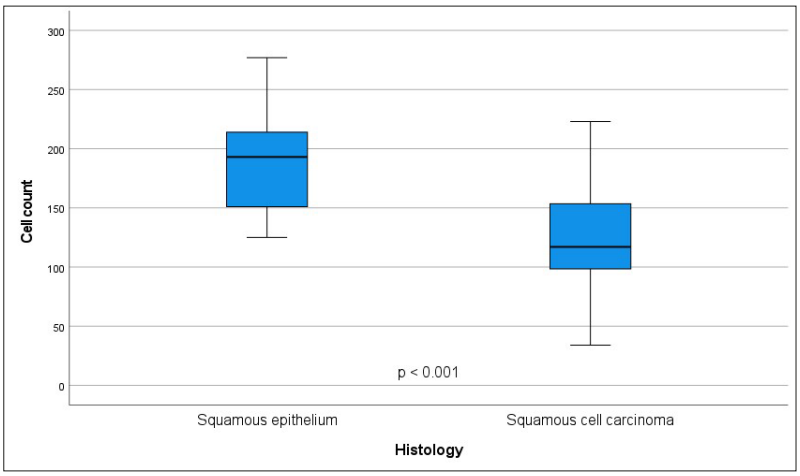

Figure 2. Detected cell count in CLE scans of squamous epithelium and the squamous cell carcinoma.

of various dimensions, sometimes with areas of necrosis and peritumoral inflammation[17]. Most proposed scoring systems for evaluating CLE images consider the alterations in cell architecture and variability of cell size[12-14]. However, an objective analysis of this feature has not yet been performed to the best of our knowledge. Our semi-automated analysis finds tumor cells to be generally larger than healthy epithelial cells (171.9±82.0 µm^2 *vs.* 246.3±171.9 µm^2, $p<0.05$).

Additionally, tumor cells show, in line with known histopathological characteristics, greater variability in size, as shown by the significantly higher standard deviation. Consequently, the cell density in a fixed field of view was found to be smaller in carcinoma with a reduced cell count (124.8±38.6 cells in SCC, 188.7±38.3 cells in images of the normal epithelium ($p<0.001$; Figure 1). The interrater variability is the most criticized aspect of CLE, which hinders its broad application outside the experimental setting. We showed in previous studies[12,13,18] that this disadvantage could be mitigated through classification systems, which consider the somewhat subjective examination of its features in a scoring system: tissue homogeneous/inhomogeneous, aberrant capillaries, and cell size variability. In previous research[15,16] we demonstrated that tissue homogeneity and aberrant capillaries could be objectively determined by the software application Cellvizio Viewer (Mauna Kea, Paris, France). We aimed to complete our assessment of each scoring system's individual features by showing significant cell size differences and variability differences by

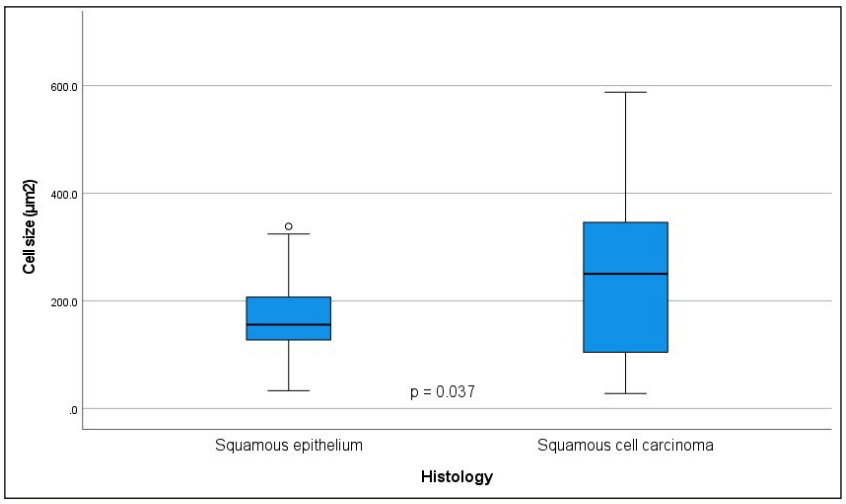

Figure 3. Measured cell sizes in CLE scans of squamous epithelium and the squamous cell carcinoma.

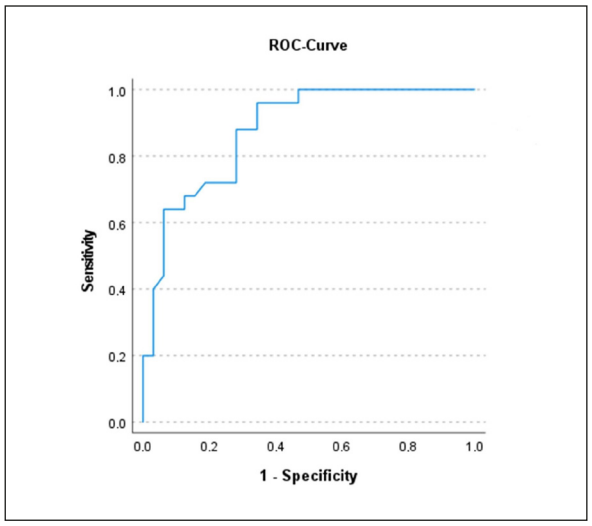

Figure 4. Receiver operating characteristic curves regarding cell density.

using an automatic cell count software (ImageJ Analysis software). This data not only increases the objectivity and interrater independency of CLE but also confirms the validity of the chosen criteria for the proposed classification systems[12,13,18].

Similar to tissue homogeneity, cell size and variability can be susceptible to motion artifacts[16]. These can cover the whole image or some sections resulting in cells appearing stretched and, therefore, larger. This issue can easily be ignored by the clinicians performing CLE in the intended setting, i.e., real-time, *in vivo*, for evaluation during or before oncologic surgery, as the movement of the probe relative to the underlying tissue can easily be perceived. Machine learning algorithms can also recognize motion artifacts with high accuracy[19]. Similarly to the effects on tissue homogeneity, artifacts such as air bubbles, blood, saliva, and debris on the surface of the probe can also taint the quality of the images and affect cell count, but this is easy to identify and discard by the surgeon in the real-time examination[15]. The integration of all these features is currently in development.

This is the first-time cell count and cell size have been examined in head and neck cancer using automated methods. *In vivo* cytometry using confocal laser microscopy has been emerging in the last few years in ophthalmology to characterize cell architecture, density, and count in corneal epithelium[20,21]. As already discussed in previous publications[22,23], the fixed depth of examination of 60 µm does not enable the differentiation of carcinoma *in situ* from carcinoma since the basal membrane – whose infiltration defines a carcinoma – is located significantly deeper (at the very least 150-900 µm). The effect of this in clinical practice is, however, limited since both lesions must be completely removed.

A score developed by our group for larynx and pharynx, which considered tissue homogeneity, cell size, presence of cell clusters, evaluation of capillary vessels, cell size, and cell borders, showed a sensitivity and specificity of 95.1% and 86.4%[15]. A scoring system specifically for the oral region regarded intercellular gaps, cell morphology, and cell size as relevant factors in differentiating of malign/benign and showed sensitivity and specificity of 95.3% and 88.9%, respectively[24]. In a previous study[18], we showed that the scoring system for the larynx is robust enough to be applied in the oral cavity, showing its transferability and clinical relevance to the chosen diagnostic criteria, among which cell architecture plays a central role. Although these diagnostic metrics do not enable CLE to be a substitute for histopathology, they come close to the values of intraoperative frozen sections, which show accuracy levels of 98.6%-88.2%[25,26].

In a previous study[16] about the diagnostic value of intraepithelial capillary loops as well as atypical vessels in SCC diagnosis, we demonstrated that a cut-off value for vessel diameter of 30 µm enables the diagnosis of SCC with a sensitivity and specificity of, respectively, 90.6% and 71.3%. For tissue homogeneity evaluation as a standalone criterion, we obtained sensitivity and specificity of 81.8% and 86.2%, respectively[15]. Regarding cell density, by using a cut-off value of 145.5 cells/FOV, we obtained sensitivity and specificity of 88.0% and 71.9%, respectively.

While the criteria of cell density, tissue homogeneity, and vessel diameter, as standalone diagnostic features provide reasonable sensitivity and specificity values, their diagnostic metrics are still inferior to diagnostic scores that integrate all these features - 95.1% and 86.4%, respectively[15]. Future work should thus consider the combination of multiple objective features to enhance diagnostic robustness.

A further path to enhancing diagnostic robustness for inexperienced users is in the automatic derivation of quantitative features from CLE images using methods of artificial intelligence, such as deep learning. A major limitation of the study is a potential selection bias, as representative frames were manually selected from the CLE sequence. This selection process could

hence induce a subjective bias and could also be a limiting factor for utilization by inexperienced users. Deep learning-based models have proven to be usable for the diagnosis of SCC yet are criticized for being non-transparent[27]. Further, displaying potentially wrong computerized results introduced significant biases into the diagnostic decision-making[28]. Deep learning-based models could, however, be used in the quality assessment of diagnostic frames with a minor impediment to the diagnostic process.

Conclusions

Accurate, automatic analysis of cell architecture, density, and size is a potential future approach to improve the diagnostic value of CLE in distinguishing squamous cell malignancies from benign mucosa. Malignant cells are usually larger than healthy epithelium cells and show far greater variability in size. Due to the known necrosis, enlarged aberrant capillaries, and peritumoral reactions, which enlarge the intercellular gaps, cell density pro field of view on CLE examination is smaller than the normal healthy epithelium. The *in vivo*, real-time examination by the clinician performing the technique during oncological surgery mitigates some weaknesses of the automatic analysis of cell architecture in whole sequences, such as motion artifacts, saliva, blood, and debris, which can be directly identified as the cause for stretched or enlarged cells. In addition, CLE enables the depiction of other criteria, which, when considered, can provide a higher diagnostic value as a single-criterion examination considering only cell density and size.

Authors' Contributions

M.S.: Conceptualization, Methodology, Software, Validation, Formal analysis, Writing - Original Draft, Visualization, Data curation, performed the experiments and collected data. M.A.: Conceptualization, Methodology, Validation, Writing–Review and Editing, Supervision. M.E.: Data curation, Review, Writing of the Manuscript. K.M.: Data curation, Review, Writing of the Manuscript. S.K.M.: Data curation, Review, Writing of the Manuscript. AO. G.: Data curation, Review, Writing of the Manuscript. M.K.: Writing - Review and Editing. H.I.: Writing - Review and Editing. M.G.: Conceptualization, Methodology, Validation, Investigation, Funding acquisition, Data Curation, Writing–Original Draft, Writing–Review and Editing, Supervision, Project administration.

Conflict of Interest

None of the authors has a personal conflict of interest to declare.

Ethics Approval

All procedures performed in this study involving human participants were following the ethical standards of the institutional and/or national research committee and with the 1964 Helsinki declaration and its later amendments or comparable ethical standards. Ethical approval (approval number 60_14 B) was given by the Non-Intervention Clinical Research Ethics Committee of the Medical Faculty of FAU Erlangen-Nürnberg.

Informed Consent

A formal informed consent procedure was obtained from all study participants.

Funding

This project was supported by Deutsche Forschungsgemeinschaft (DFG, German Research Foundation) grant number GO 3182/2-1, Project Number 439264659.

Availability of Data and Materials

The data that support the findings of this study are available from the corresponding author upon reasonable request.

ORCID ID

Miguel Goncalves: 0000-0002-0036-4598

References

1) Jones TM, De M, Foran B, Harrington K, Mortimore S. Laryngeal cancer: United Kingdom National Multidisciplinary guidelines. J Laryngol Otol 2016; 130: 75-82.
2) Bootz F. S3-Leitlinie Diagnostik, Therapie und Nachsorge des Larynxkarzinoms [Guideline on diagnosis, treatment, and follow-up of laryngeal cancer]. HNO 2020; 68: 757-762.
3) Al Afif A, Rigby MH, MacKay C, Brown TF, Phillips TJ, Khan U, Trites JRB, Corsten M, Taylor SM. Injection laryngoplasty during transoral larolled trial. J Otolaryngol Head Neck Surg 2022; 51: 12.
4) De Leeuw F, Abbaci M, Casiraghi O, Ben Lakhdar A, Alfaro A, Breuskin I, Laplace-Builhé C. Value of Full-Field Optical Coherence Tomography Imaging for the Histological Assessment of Head and Neck Cancer. Lasers Surg Med 2020; 52: 768-778.

5) Sievert M, Mantsopoulos K, Mueller SK, Eckstein M, Rupp R, Aubreville M, Stelzle F, Oetter N, Maier A, Iro H, Goncalves M. Systematic interpretation of confocal laser endomicroscopy: larynx and pharynx confocal imaging score. Acta Otorhinolaryngol Ital 2022; 42: 26-33.
6) Li Z, Li Z, Chen Q, Zhang J, Dunham ME, McWhorter AJ, Feng JM, Li Y, Yao S, Xu J. Machine-learning-assisted spontaneous Raman spectroscopy classification and feature extraction for the diagnosis of human laryngeal cancer. Comput Biol Med 2022; 146: 105617.
7) Sun C, Han X, Li X, Zhang Y, Du X. Diagnostic Performance of Narrow Band Imaging for Laryngeal Cancer: A Systematic Review and Meta-analysis. Otolaryngol Head Neck Surg 2017; 156: 589-597.
8) Goncalves M, Aubreville M, Mueller SK, Sievert M, Maier A, Iro H, Bohr C. Probe-based confocal laser endomicroscopy in detecting malignant lesions of vocal folds. Acta Otorhinolaryngol Ital 2019; 39: 389-395.
9) Kakaletri I, Linxweiler M, Ajlouni S, Charalampaki P. Development, Implementation and Application of Confocal Laser Endomicroscopy in Brain, Head and Neck Surgery-A Review. Diagnostics (Basel) 2022; 12: 2697.
10) Sievert M, Auberville M, Oetter N, Stelzle F, Maier A, Mantsopoulos K, Iro H, Goncalves M. Konfokale Laser-Endomikroskopie des Kopf-Hals-Plattenepithelkarzinoms: eine systematische Übersicht [Confocal laser endomicroscopy of head and neck squamous cell carcinoma: a systematic review]. Laryngorhinootologie 2021; 100: 875-881.
11) Abbaci M, Dartigues P, De Leeuw F, Soufan R, Fabre M, Laplace-Builhé C. Patent blue V and indocyanine green for fluorescence microimaging of human peritoneal carcinomatosis using probe-based confocal laser endomicroscopy. Surg Endosc 2016; 30: 5255-5265.
12) Sievert M, Mantsopoulos K, Mueller SK, Eckstein M, Rupp R, Aubreville M, Stelzle F, Oetter N, Maier A, Iro H, Goncalves M. Systematic Interpretation of Confocal Laser endomicroscopy: Larynx and Pharynx Confocal Imaging Score. Acta Otorhinolaryngol Ital 2021; 42: 26-33.
13) Sievert M, Mantsopoulos K, Mueller SK, Rupp R, Eckstein M, Stelzle F, Oetter N, Maier A, Aubreville M, Iro H, Goncalves M. Validation of a classification and scoring system for the diagnosis of laryngeal and pharyngeal squamous cell carcinomas by confocal laser endomicroscopy. Braz J Otorhinolaryngol 2021; 88: 26-32.
14) Nathan CA, Kaskas NM, Ma X, Chaudhery S, Lian T, Moore-Medlin T, Shi R, Mehta V. Confocal Laser Endomicroscopy in the Detection of Head and Neck Precancerous Lesions. Otolaryngol Head Neck Surg 2014; 151: 73-80.
15) Sievert M, Aubreville M, Gostian AO, Mantsopoulos K, Koch M, Mueller SK, Eckstein M, Rupp R, Stelzle F, Oetter N, Maier A, Iro H, Goncalves M. Validity of tissue homogeneity in confocal laser endomicroscopy on the diagnosis of laryngeal and hypopharyngeal squamous cell carcinoma. Eur Arch Otorhinolaryngol 2022; 279: 4147-4156.
16) Sievert M, Eckstein M, Mantsopoulos K, Mueller SK, Stelzle F, Aubreville M, Oetter N, Maier A, Iro H, Goncalves M. Impact of intraepithelial capillary loops and atypical vessels in confocal laser endomicroscopy for the diagnosis of laryngeal and hypopharyngeal squamous cell carcinoma. Eur Arch Otorhinolaryngol 2022; 279: 2029-2037.
17) Ciolofan MS, Vlăescu AN, Mogoantă CA, Ioniță E, Ioniță I, Căpitănescu AN, Mitroi MR, Anghelina F. Clinical, Histological and Immunohistochemical Evaluation of Larynx Cancer. Curr Health Sci J 2017; 43: 367-375.
18) Sievert M, Oetter N, Mantsopoulos K, Gostian AO, Mueller SK, Koch M, Balk M, Thimsen V, Stelzle F, Eckstein M, Iro H, Goncalves M. Systematic classification of confocal laser endomicroscopy for the diagnosis of oral cavity carcinoma. Oral Oncol 2022; 132: 105978.
19) Aubreville M, Stoeve M, Oetter N, Goncalves M, Knipfer C, Neumann H, Bohr C, Stelzle F, Maier A. Deep learning-based detection of motion artifacts in probe-based confocal laser endomicroscopy images. Int J Comput Assist Radiol Surg 2019; 14: 31-42.
20) Sterenczak KA, Winter K, Sperlich K, Stahnke T, Linke S, Farrokhi S, Klemm M, Allgeier S, Köhler B, Reichert KM, Guthoff RF, Bohn S, Stachs O. Morphological characterization of the human corneal epithelium by in vivo confocal laser scanning microscopy. Quant Imaging Med Surg 2021; 11: 1737-1750.
21) Colorado LH, Alzahrani Y, Pritchard N, Efron N. Assessment of conjunctival goblet cell density using laser scanning confocal microscopy versus impression cytology. Cont Lens Anterior Eye 2016; 39: 221-226.
22) Arens C, Glanz H, Wönckhaus J, Hersemeyer K, Kraft M. Histologic assessment of epithelial thickness in early laryngeal cancer or precursor lesions and its impact on endoscopic imaging. Eur Arch Otorhinolaryngol 2007; 264: 645-649.
23) Armstrong WB, Ridgway JM, Vokes DE, Guo S, Perez J, Jackson RP, Gu M, Su J, Crumley RL, Shibuya TY, Mahmood U, Chen Z, Wong BJ. Optical coherence tomography of laryngeal cancer. Laryngoscope 2006; 116: 1107-1113.
24) Oetter N, Knipfer C, Rohde M, von Wilmowsky C, Maier A, Brunner K, Adler W, Neukam FW, Neumann H, Stelzle F. Development and validation of a classification and scoring system for the diagnosis of oral squamous cell carcinomas through confocal laser endomicroscopy. J Transl Med 2016; 14: 159.
25) Layfield EM, Schmidt RL, Esebua M, Layfield LJ. Frozen Section Evaluation of Margin Status in Primary Squamous Cell Carcinomas of the Head and Neck: A Correlation Study of Frozen Section and Final Diagnoses. Head Neck Pathol 2018; 12: 175-180.
26) Kubik MW, Sridharan S, Varvares MA, Zandberg DP, Skinner HD, Seethala RR, Chiosea SI. Intraoperative Margin Assessment in Head and Neck

Cancer: A Case of Misuse and Abuse? Head Neck Pathol 2020; 14: 291-302.

27) Aubreville M, Knipfer C, Oetter N, Jaremenko C, Rodner E, Denzler J, Bohr C, Neumann H, Stelzle F, Maier A. Automatic Classification of Cancerous Tissue in Laserendomicroscopy Images of the Oral Cavity using Deep Learning. Sci Rep 2017; 20: 11979.

28) Marzahl C, Bertram CA, Aubreville M, Petrick A, Weiler K, Gläsel AC, Maier A. Are fast labeling methods reliable? A case study of computer-aided expert annotations on microscopy slides. Published in: Medical Image Computing and Computer Assisted Intervention – MICCAI 2020. Springer, Cham, 2020; 24-34.